Journal of Alloys and Compounds 890 (2021) 161847

Contents lists available at ScienceDirect

Journal of Alloys and Compounds

journal homepage: www.elsevier.com/locate/jalcom

Large magnetocaloric effect in $EuGd_2O_4$ and $EuDy_2O_4$

E. Palacios[a,b,*], R. Sáez-Puche[c], J. Romero[c], Y. Doi[d], Y. Hinatsu[d], M. Evangelisti[a,b,*]

[a] Instituto de Nanociencia y Materiales de Aragón (INMA), CSIC–Universidad de Zaragoza, 50009 Zaragoza, Spain
[b] Departamento de Física de la Materia Condensada, Universidad de Zaragoza, 50009 Zaragoza, Spain
[c] Departamento de Química Inorgánica, Universidad Complutense de Madrid, 28040 Madrid, Spain
[d] Graduate School of Science, Hokkaido University, Sapporo 060-0810, Japan

ARTICLE INFO

Article history:
Received 10 June 2021
Received in revised form 29 July 2021
Accepted 1 September 2021
Available online 7 September 2021

Keywords:
Magnetically ordered materials
Rare-earth alloys and compounds
Magnetocaloric
Calorimetry
Magnetic measurements

ABSTRACT

Magnetization, heat capacity and direct measurements of the magnetocaloric effect show that $EuGd_2O_4$ and $EuDy_2O_4$ have a remarkably large magnetocaloric effect at cryogenic temperatures, owing to their high magnetic density and low ordering temperatures. The Gd derivative orders antiferromagnetically at T_N = 4.6 K, while its magnetocaloric effect largely exceeds that of *the* reference refrigerant Gadolinium Gallium Garnet (GGG) above 5 K. The Dy derivative undergoes two phase transitions at T_{C1} = 3.65 K and T_{C2} = 4.7 K, respectively, which are the result of a peculiar magnetic arrangement: the first Dy sublattice is parallel to the crystallographic *c*-axis, while the Eu sublattice makes a variable angle from 0^o to 45^o with the direction of the second Dy sublattice that lies in the *ab*-plane. $EuDy_2O_4$ has a lower magnetocaloric effect than $EuGd_2O_4$, yet larger than GGG. Both ordering mechanisms are semi-quantitatively explained within the frame of a mean-field simulation, which takes into account the magnetic anisotropy strength of the participating magnetic ions.

1. Introduction

Magnetic ordering determines how magnetic entropy is released as a function of temperature and applied magnetic field. By properly synthesizing and/or selecting materials and their constituent elements, one can adjust the magnetic interaction and anisotropy in order to optimize the magnetocaloric effect (MCE) for the working temperatures of the target application. A ferromagnet is the most evident case, since a weak or moderate applied magnetic field produces a large change in the isothermal entropy variation ΔS_T near its Curie temperature T_C. In the paramagnetic state and for a weak external magnetic field variation from zero to B, ferromagnetic correlations lead to $\Delta S_T \simeq -(1/2)CB^2/(T-T_C)^2$, where C is the Curie constant [1]. These entropy variations are larger than that produced by the absence of magnetic interactions, i.e., in the limit of magnetically diluted spins. As an example case of a ferromagnet at cryogenic temperatures, EuS orders at T_C = 16 K and has a remarkable maximum isothermal entropy increment $|\Delta S_{T,max}| \simeq 54$ Jkg^{-1}K^{-1} for B = 8 T [2–4]. Unfortunately and inherently to any ferromagnet, the MCE diminishes drastically at temperatures well below T_C as the magnetization becomes spontaneously saturated, hence inhibiting application at low temperatures. An interesting and yet poorly explored situation is when two sublattices coexist, of which only one orders ferromagnetically at relatively high temperature. Besides any external B, the paramagnetic sublattice experiences also the internal field generated by the ferromagnetic exchange, hence resulting in an effective enhancement of the MCE. As an example of such polarization, $GdCrO_4$ has $|\Delta S_T| > 20$ Jkg^{-1}K^{-1} between relatively low 5 K and up to 35 K, for B = 9 T [5,6].

Antiferromagnetism has a somewhat similar, but worse, behavior than ferromagnetism, although it can open a different avenue for attaining a large MCE at low temperatures. Below the antiferromagnetic critical temperature T_N, $|\Delta S_T|$ diminishes similarly as for a ferromagnet, even inverting sign ($\Delta S_T > 0$) for B smaller than the spin-flop transition field and applied parallel to the magnetic ordering direction. In the paramagnetic state and for weak B, antiferromagnetic correlations also reduce the MCE [7], as they lead to $\Delta S_T \simeq -(1/2)CB^2/(T+\theta)^2$, where θ is the Curie-Weiss temperature. However, antiferromagnetic coupling can be particularly desirable when all antiferromagnetic interactions present in the spin system cannot be simultaneously satisfied, resulting in spin frustration [8]. The Curie-Weiss temperature of a geometrically frustrated magnet can be significantly larger than T_N, that is, frustration can extend the temperature range of paramagnetic-like behavior. This can ultimately facilitates large MCE at low temperature [9–12–15].

* Corresponding authors at: Instituto de Nanociencia y Materiales de Aragón (INMA), CSIC–Universidad de Zaragoza, 50009 Zaragoza, Spain.
E-mail addresses: elias@unizar.es (E. Palacios), m.e@csic.es (M. Evangelisti).

https://doi.org/10.1016/j.jallcom.2021.161847
0925-8388/

Gadolinium Gallium Garnet (GGG), i.e. $Gd_3Ga_5O_{12}$, is an archetypal frustrated magnet, in addition to being *the* reference magnetic refrigerant material because of its strong MCE between ca. 1 K and 10 K, which is routinely exploited in commercial demagnetization refrigerators. In spite of having a relatively large magnetic density and antiferromagnetic correlation strength of $\theta \approx 2$ K, GGG shows no magnetic phase transition down to ≈25 mK under zero applied magnetic field [16]. In GGG, $|\Delta S_T|$ reaches 39 $Jkg^{-1}K^{-1}$ for $B = 5$ T and $T = 2.55$ K, although it decays significantly at higher temperatures, e.g., 15 $Jkg^{-1}K^{-1}$ at 10 K and 5.3 $Jkg^{-1}K^{-1}$ at 20 K [17].

The isostructural family of rare-earth ferrite-type AR_2O_4 compounds (A = Sr, Ba; R = rare earth or Y) is another example of a frustrated spin system [18–21–24,25]. Its structure consists of ladders of triangular rungs made of R^{3+} ions. An interesting possibility for increasing the magnetic density of this spin system is by replacing the alkaline-earth element by Eu^{2+}, which ultimately leads to long-range ordering temperatures below 5 K [26]. Eu^{2+} has the same electron configuration and magnetic behavior of Gd^{3+}, which is often present in magnetocaloric materials because of its zero orbital angular momentum and largest entropy per single ion. However, Eu^{2+} and Gd^{3+} differ drastically to one another as regards their chemical properties. Eu^{2+} has a larger ionic radius $r_i(Eu^{2+}) = 1.17$ Å (for coordination VI), comparing to $r_i(Gd^{3+}) = 1.08$ Å, and different charge, allowing Eu^{2+} to be at crystal sites where Gd^{3+} cannot. Therefore, the so-obtained EuR_2O_4 is potentially very attractive in terms of MCE. Hereafter, we focus on $EuGd_2O_4$ and $EuDy_2O_4$, for which we present direct and indirect measurements of their MCE, namely magnetization and heat capacity. These two compounds represent the extremes of low and high magnetic anisotropy, respectively, which ultimately explains the very different experimental results. Anticipating some of the results, $EuGd_2O_4$ orders antiferromagnetically, although it presents dominant ferromagnetic correlations (negative θ) that produce a relatively large MCE also in the paramagnetic state. The behavior of the Dy compound is accounted for by two perpendicular Dy sublattices, similar as it occurs in $SrDy_2O_4$ [27]. For both sublattices, each Dy^{3+} ion carries an Ising $s = 1/2$ pseudo-spin with a moment of 10 μ_B. The isotropic Eu^{2+} ions are polarized by both Dy sublattices. A simplified mean-field calculation supports these pictures. Overall, both materials show very large values of cryogenic MCE, especially the Gd derivative.

This paper is organized as follows. Section 3 provides a brief description of rare-earth ferrite-type compounds. Section 4 combines results of magnetization M and direct-current magnetic susceptibility χ. Section 5 is devoted to heat capacity at constant magnetic field and zero pressure, $C_{p,B}$, and to the entropy deduced from it. Section 6 deals with the MCE, deduced from magnetization and heat capacity data, and directly measured. Finally, A describes the original technique we employ to determine directly ΔS_T and B describes the mean-field calculations.

2. Experimental methods

2.1. Sample preparation and structural characterization

Samples of $EuGd_2O_4$ and $EuDy_2O_4$ were prepared according to a procedure that some of us described in Ref. [26]. We verified that the compounds had the expected crystal structure by X-ray powder diffraction on a Philips X'Pert PRO ALPHA 1 (Panalytical) instrument, equipped with a Germanium monochromator (Cu $K\alpha_1$); data were collected from $2\theta = 10^\circ$ to 110°, with a step of 0.017°, over a period of 12 h.

2.2. Magnetization and magnetothermal measurements

Isothermal direct-current (DC) magnetization data were collected for powder samples, using a Quantum Design Physical Property Measurement System (PPMS), for temperatures T down to 2 K and applied magnetic fields B up to 9 T. The relative error in the measurements is lower than 1%. The samples have a shape of a cylinder with a length-to-diameter ratio of approximately 3, corresponding to a demagnetizing factor $N_d \simeq 0.13$, taken into account for estimating the real field acting on the sample: $\mu_0 H = B - N_d \mu_0 M_V$, where M_V is the magnetic moment per unit of volume.

The heat capacity $C_{p,B}$ was measured by the relaxation method at constant magnetic fields from 0 to 9 T, using a PPMS. The sample was in the form of flat cylinder of compressed powder tablet. The magnetic field was applied parallel to the base of the tablet to minimize overheating by eddy currents in the measuring system (the samples are electrically insulators). The corresponding higher demagnetization factor of $N_d \simeq 0.2$, with respect to that used for the magnetic measurements, produces systematically slight differences in the magnetocaloric parameters deduced from heat capacity when compared with those deduced from magnetization.

Direct measurements of the isothermal entropy variation ΔS_T were performed using a sapphire plate to which a Cernox (CX-1010) resistance thermometer was attached, installed in the same PPMS setup employed for heat capacity. As per the heat capacity measurements, the sample consisted of a pressed pellet and the magnetic field was applied parallel to the plate to minize overheating by eddy currents. A provides further details on this measuring technique.

3. Rare-earth ferrite-type compounds

The AR_2O_4 compounds (A = Sr, Ba, R = rare earth or Y) have the crystal structure of orthorhombic CaV_2O_4 (Fig. 1) or that of ferrite $CaFe_2O_4$, space group *Pnam*, with $c \ll a$, b [22]. There are two inequivalent sites in the asymmetric unit for the R atoms, named after Ref. [18] as $R1$ at position (0.42, 0.11, 1/4) and $R2$ at (0.42, 0.61, 1/4), in units of the cell parameters. Both atoms $R1$ and $R2$ form separately ladders made of rungs with a triangular arrangement in which the distance between first and second neighbors is almost equal (Fig. 1). Also the exchange between nearest and next-nearest neighbors has similar magnitude. The interaction in the V or R compounds is antiferromagnetic. Therefore, this system is highly frustrated. Because of the frustration and the low dimensionality, these compounds order at very low temperatures or do not order at all within the investigated temperatures. For example, $BaGd_2O_4$ orders antiferromagnetically at $T_N = 2.6$ K [19]. As a further example, $SrGd_2O_4$ orders at 2.73 K [28], and has a large MCE of up to $|\Delta S_{T,max}| = 27$ $Jkg^{-1}K^{-1}$ at 3 K, for a magnetic field increment from 0 to 7 T [25].

Some of us [26] have synthesized EuR_2O_4 with R = G*d* and other rare-earth elements, from Dy to Lu. All of these compounds have the CaV_2O_4 structure, with very similar structural parameters and magnetic ordering temperatures ranging from 4.7 K for R = H*o* to 6.3 K for R = Y*b*. Because of the presence of non-magnetic Lu^{3+}, $EuLu_2O_4$ allows to single out the interactions between the Eu^{2+} ions. The Eu^{2+} ions form chains parallel to the crystallographic c-axis, having an intra-chain distance of 3.34 Å that is significantly shorter than the distance of 5.50 Å between nearest chains. The paramagnetic susceptibility follows the Curie-Weiss behavior $\chi = C/(T + \theta)$ with $\theta \simeq -3.6$ K, indicating dominant ferromagnetic correlations (see Fig. 8-a in Ref. [26]). However, the long-range magnetic order that takes place below $T_N = 5.7$ K is antiferromagnetic. The proposed magnetic structure consists of antiparallel-aligned ferromagnetic chains of Eu^{2+} ions, with moments pointing along the c-axis [26].

4. Magnetization and magnetic susceptibility

Figs. 2 and 3 show the temperature-dependencies of the molar magnetization M and magnetic susceptibility $\chi_m = M/H$ for $EuGd_2O_4$

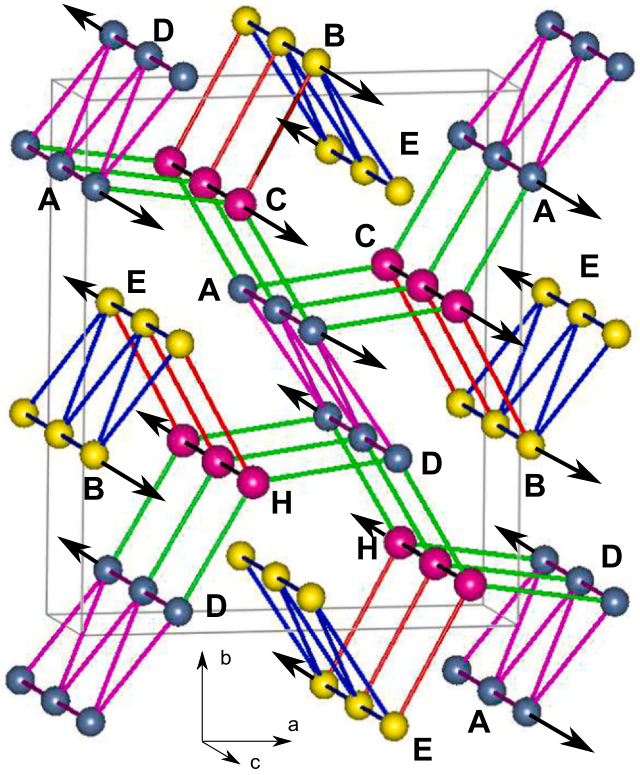

Fig. 1. Structure of EuR_2O_4, according to parameters refined from powder X-ray diffraction data, together with the antiferromagnetic spin configuration in six sublattices, as proposed for $R = Gd$ at low temperature (see Section 7.1). Oxygen atoms, at intermediate sites between metal ions, are omitted for clarity. Shortest distances are indicated by links. Color code for individual atoms: Eu, red; *R*1, yellow; *R*2, blue. Color code for distances: Eu-Eu, black; Eu-*R*1, red; Eu-*R*2, green; *R*1 – *R*1, blue; *R*2 – *R*2, magenta. The blue and magenta links show the arrangement of *R*1 and *R*2 in two similar but symmetry independent ladders of triangular rungs.

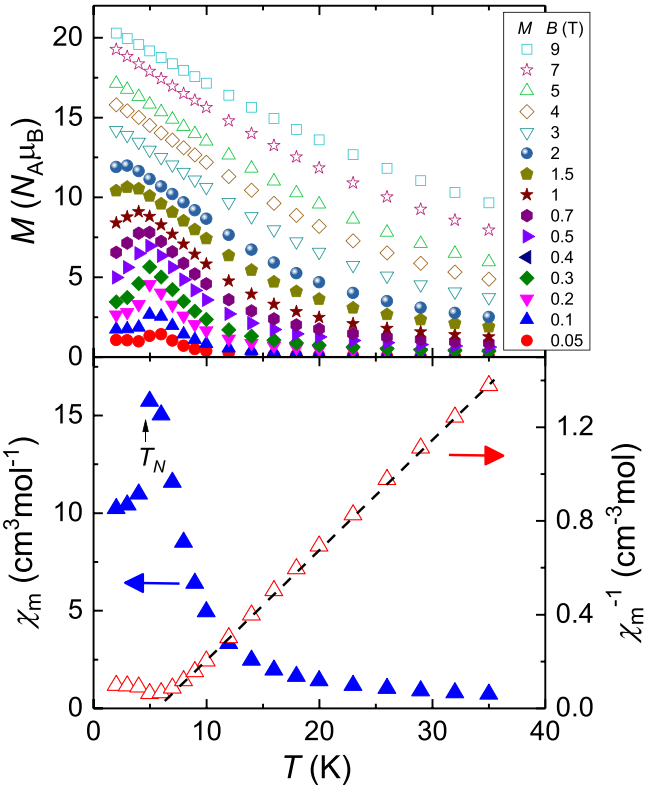

Fig. 2. For $EuGd_2O_4$, temperature-dependence of the molar magnetization *M* (top) for selected *B* values, as labelled, and the molar magnetic susceptibility χ_m (bottom, filled symbols) and its inverse (bottom, open symbols), collected for a DC applied magnetic field of 0.1 T. Shown also is the fit to the Curie-Weiss law (dashed line), in addition to the phase transition temperature, as obtained from the heat capacity data (Section 5).

and $EuDy_2O_4$, respectively. For both compounds and low fields, *M* increases on descending temperature until a maximum is reached near the temperatures where long-range magnetic order takes place (T_N = 4.6 K for $EuGd_2O_4$, T_{C1} = 3.65 K and T_{C2} = 4.7 K for $EuDy_2O_4$, see Section 5).

4.1. $EuGd_2O_4$

Below T_N, the susceptibility measured for 0.1 T decreases down to 2/3 of the maximum (Fig. 2), in accord with the value expected for a powder sample with random orientation of the grains. For fields higher than 3 T, *M* does not decrease at low temperature. This fact is interpreted as due to a transition from antiferromagnetic to spin-flop state at low temperatures. Due to the weak anisotropy of Gd the spin-flop transition occurs at moderate values of the field. Magnetization reaches the saturation of $M = 21 N_A \mu_B$ at low temperatures and high fields.

Above 10 K, the susceptibility of $EuGd_2O_4$ follows the Curie-Weiss dependence $\chi_m = C/(T+\theta)$ with $\theta = -5.9$ K and $C = 21.8\ cm^3 K mol^{-1}$, which compares well with the value expected for three non-interacting $s = 7/2$ spins per formula unit, i.e., $3s(s+1)g^2 N_A \mu_B^2/(3k_B) = 23.6\ \ cm^3 K mol^{-1}$ (Fig. 2). The negative value of θ indicates dominant ferromagnetic correlations in the paramagnetic phase, which happen to be stronger than the Eu-Eu interaction in $EuLu_2O_4$ [26]. Considering that the *R*-*R* interaction in SrR_2O_4 and BaR_2O_4 is antiferromagnetic (see Section 3), one has to conclude that the presence of Gd^{3+} ions should enhance the ferromagnetic Eu-Eu interaction in $EuGd_2O_4$. However, the Eu-Eu interaction promotes quasi-one-dimensional ferromagnetic fluctuations and, therefore, it cannot solely account for the phase transition. On decreasing temperature, when the intrachain correlation length is high enough, a weak interchain interaction would align the chains antiparallel, giving the antiferromagnetically ordered configuration.

4.2. $EuDy_2O_4$

At low temperature, *M* decays for all fields up to 7 T (Fig. 3). This different behavior, with respect to the Gd compound, is interpreted as due to the high magnetic anisotropy. Crystal-field levels of two inequivalent Dy^{3+} ions have been determined for $SrDy_2O_4$ by inelastic neutron scattering [27]. We assume the same values for $EuDy_2O_4$, because the nearest-neighboring O^{2-} ions are at very similar positions in both materials. For Dy1 (Dy2), the first excited doublet is 4 m*eV* = 46.4 K (29 m*eV* = 333.6 K) above the ground doublet. Both values are much higher than any temperature and energy considered here. Therefore, a spin-flip transition should be expected to occur in $EuDy_2O_4$, that is, a direct transition from antiferromagnetic to paramagnetic phase with increasing parallel field, without any intermediate spin-flop phase. A rough estimate of the spin-flip field B_{sf} can be given for $T \to 0$. Simplifying to a pair of collinearly ordered Dy^{3+} moments μ and considering zero exchange energy when the spins are randomly oriented, the spin flip occurs when the sum of the Zeeman and exchange energy of the antiferromagnetic state ($E_{\uparrow\downarrow} = +\mu B_{sf} - \mu B_{sf} - E_{exch} = -E_{exch}$) equals that of the spin-flipped configuration ($E_{\uparrow\uparrow} = -2\mu B_{sf} + E_{exch}$), that is, $\mu B_{sf} = E_{exch}$. Assuming $E_{exch} \simeq k_B T_N$, we obtain $B_{sf} \simeq 0.7$ T for a magnetic moment $\mu = 10\mu_B$, taken from the closely related pyrochlores [29].

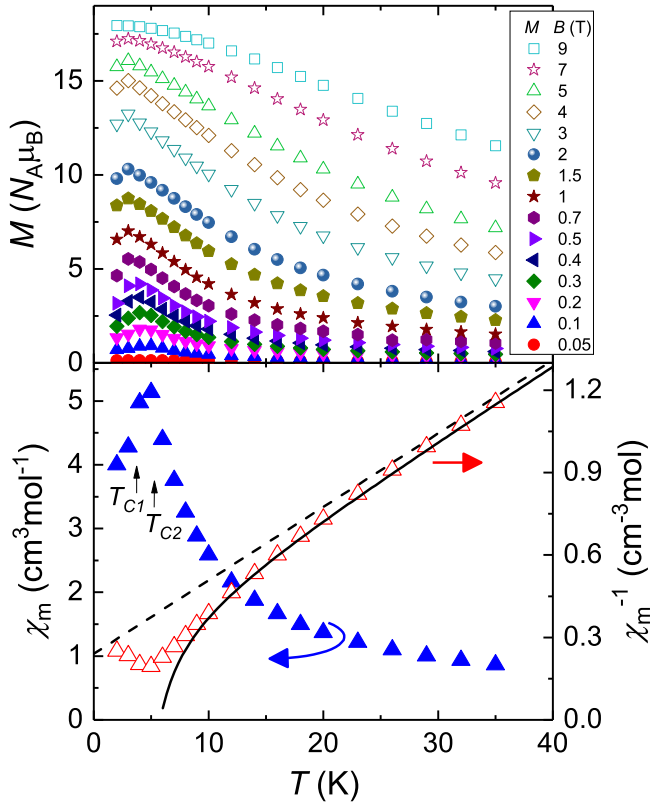

Fig. 3. For $EuDy_2O_4$, temperature-dependence of the molar magnetization M (top) for selected B values, as labelled, and the molar magnetic susceptibility χ_m (bottom, filled symbols) and its inverse (bottom, open symbols), collected for a DC applied magnetic field of 0.1 T. Shown also are the fits to the Curie-Weiss (dashed line) and Neel-type hyperbolic (solid line) laws, in addition to the phase transition temperatures, as obtained from the heat capacity data (Section 5).

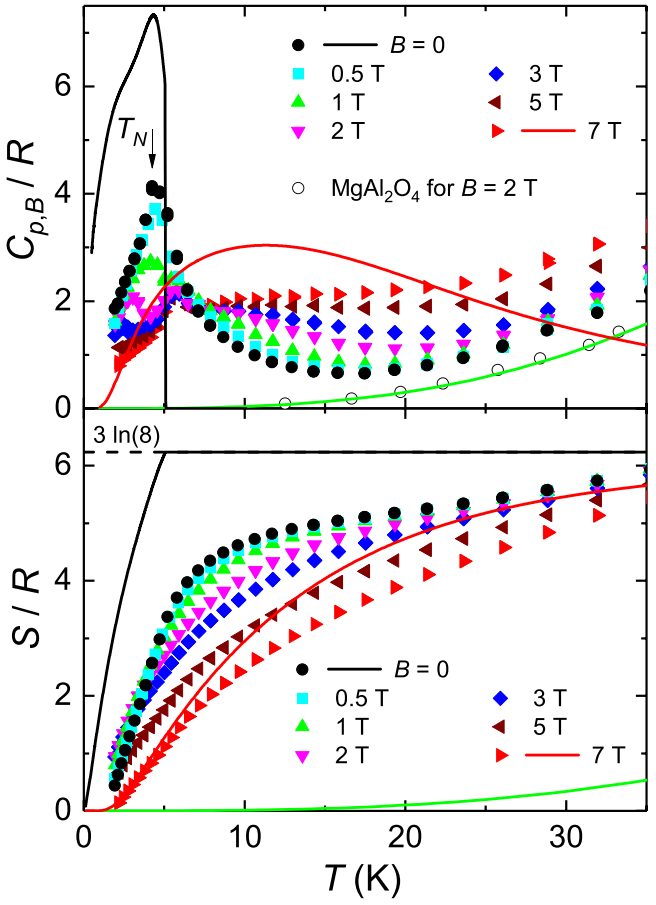

Fig. 4. Temperature-dependence of the molar heat capacity (top) and molar entropy (bottom) of $EuGd_2O_4$, collected for several applied magnetic fields, as labelled. Shown also are the lattice contributions, as obtained from $MgAl_2O_4$ (open symbols) and calculated from the Debye model for $T_D = 351$ K (green lines), together with the mean-field calculations for $B = 0$ (black lines) and 7 T (red lines). The dashed line is the high-temperature limit of the magnetic entropy for three $s = 7/2$ spins per formula unit, i.e., $S_m(T \to \infty)/R = 3\ln(8)$.

This value compares well with, e.g., $B_{sf} = 0.57$ T reported for $DyPO_4$ that has a similar long-range ordering temperature [30]. Because of the random orientation of the grains in powder sample, only one component of external B triggers the spin-flip transition for each grain. We observe that applied fields of up to 7 T are not sufficient for all grains and a fraction of them still remain in the antiferromagnetic phase, causing the decrease of M with lowering T at the lowest temperatures. Furthermore, anticipating Section 7, the Dy1 and Dy2 sublattices order perpendicularly with respect to one another. For this reason, and because of the random orientation of the grains, the expected saturation magnetization of $\approx 27 N_A \mu_B$ is never reached experimentally.

In the paramagnetic state, the susceptibility of $EuDy_2O_4$ behaves as that of a ferrimagnet and can be fit to the Néel-type hyperbola $1/\chi_m = (T + \theta)/C - \zeta/(T - \theta')$ [31]. At high temperatures, the net magnetization and the molecular field are weak. Spins are polarized parallel to an external field, although the antiferromagnetic interaction between them reduces the susceptibility with respect to a paramagnet. At lower temperatures but still above θ', the spins align antiparallel with an external magnetic field (see B.1 for the corresponding mean-field calculation), while still giving a net moment. At $T_C = \theta'$, $1/\chi_m$ is expected to drop to zero. The Néel-type hyperbola is plotted in Fig. 3 along with the experimental data, for $\theta = 9$ K, $C = 37.5$ cm^3Kmol^{-1}, $\zeta = 0.9$ $cm^{-3}K^{-1}mol$ and $\theta' = 3.5$ K. The Curie-Weiss law for $\theta = 9$ K and $C = 37.5$ cm^3Kmol^{-1} is also plotted, for comparison. Note that the behavior of $1/\chi_m$ for $T \to \infty$ gives the Curie constant C, which is about one half of the value expected for one Eu^{2+} spin $s_1 = 7/2$, $g_1 = 2$ and two Dy^{3+} Ising pseudo-spins $s_2 = 1/2$, $g_2 = 20$ per formula unit, i.e., $[g_1^2 s_1(s_1+1) + 2g_2^2 s_2(s_2+1)]N_A\mu_B^2/(3k_B) = 82.8$ cm^3Kmol^{-1}. This large discrepancy can be explained by taking into account that the susceptibility of a powder sample is $(\chi_\parallel + 2\chi_\perp)/3 \simeq \chi_\parallel/3$, where $\chi_\parallel$ and $\chi_\perp$ are the parallel and perpendicular components, respectively, and that Dy1 and Dy2 form two perpendicular sublattices, as discussed in Section 7. Assuming that a perpendicular applied magnetic field cannot polarize an Ising spin at all, one would then expect $C = [g_1^2 s_1(s_1+1) + (2/3)g_2^2 s_2(s_2+1))]N_A\mu_B^2/(3k_B) = 32.8$ cm^3Kmol^{-1}. The experimental value is somewhat higher, likely because $\chi_\perp$ might not be exactly zero for the Dy sublattices, especially at the high temperatures where the Curie-Weiss law is obeyed. In fact, the crystal-field excited doublet of Dy1 is at 46.4 K, indicating that the sublattice would deviate from the ideal Ising behavior near or above this temperature. Finally, it should be noted that the susceptibility of a sample having a net magnetization is limited at high values by the demagnetization field, as particularly evident at low temperatures. Therefore, the experimental $1/\chi_m$ does not reach zero, rather it decays to a minimum value, identified with the Curie temperature $T_{C2} \simeq 4.5$ K, as can be seen in Fig. 3.

5. Heat capacity

Figs. 4 and 5 show the temperature-dependencies of the heat capacity $C_{p,B}$ and entropy S for $EuGd_2O_4$ and $EuDy_2O_4$, respectively. For both compounds, we estimate the phonon contribution by using C_p of the isostructural non-magnetic compound $MgAl_2O_4$ [32], after

applying a scale factor in temperature to take into account the different atomic masses of the elements, specifically, C_{ph} (EuR_2O_4, T) ≃ C_p($MgAl_2O_4$, $2T$). Alternatively, the phonon contribution can be obtained as a Debye function $C_{V,Deb}$ with the characteristic temperature T_D ≃ 351 K, determined from the speed of sound for BaY_2O_4 [33], which is close to EuR_2O_4 in molar mass. The function $21 \times C_{V,Deb}(T/T_D)$ matches the data of C_p($MgAl_2O_4$, $2T$). From the comparison with the experimental data, it is clear that the experimental heat capacity of both compounds is essentially magnetic below 20 K because the phonon contribution is significantly smaller.

5.1. $EuGd_2O_4$

The zero-field heat capacity of $EuGd_2O_4$ (Fig. 4, top panel) has a peak at T_N = 4.6 K that can be associated with antiferromagnetic order [26,34], as also deduced in Section 4.1. This peak is not the typical lambda-type anomaly and its height is about half the value of the mean-field calculation B.2. The experimental heat capacity remains relatively large well above T_N, denoting the presence of short-range order due to the quasi-1D character of the exchange interactions between Eu^{2+} ions.

In spite of the ferromagnetic Curie-Weiss behavior, the applied magnetic field dependence of the heat capacity indicates clearly antiferromagnetic ordering below T_N. The peak is insensitive to weak fields and decreases in temperature and height for stronger fields, theoretically above the spin-flop (SF) field. The transition between the SF and paramagnetic phases at constant applied field is accompanied by a small entropy content, hence C_p has a small peak along with a round shoulder, similar to the Schottky contribution of a paramagnet in applied field. At high fields, the fading of the magnetic peak reveals the onset of another peak centered at 5.7 K that is field independent up to the maximum accessed field of 7 T. Although it occurs near the temperature of maximum susceptibility, it is difficult to ascribe it to a magnetic transition and it is likely due to an impurity in the sample.

The entropy (Fig. 4, bottom panel) has been deduced by the integration

$$S(T, B) = \int_0^T \frac{C_p(T', B)}{T'} dT'. \quad (1)$$

To determine the absolute entropy for B = 7 T, the experimental data have been extrapolated for $T \to 0$ by the mean-field calculation. Regardless, the entropy is very small at low temperatures, as expected from the magnetization that approaches saturation (Fig. 2). By making use of $S(T, 7\,T)$ and the experimental entropy differences ΔS_T, deduced from magnetization (see Section 6), we remove any uncertainty in the determination of the absolute entropy for the other applied field values.

At relatively high temperature, the zero-field entropy is lower than the expected limit $S_m(T \to \infty)/R = 3\ln(2s + 1) = 3\ln(8) = 6.24$, corresponding to three spins $s = 7/2$ per formula unit. For instance, the experiment provides $S(T, B = 0)/R$ = 5.5 ± 0.1 at $T \simeq 20$ K. The magnetic critical entropy fraction for zero field, i.e., $1 - S_m(T_N, B = 0)/S_m(T \to \infty, B = 0)$ = 0.48, is relatively large because low-dimensional magnetic fluctuations extend towards high temperature, in accord with the heat capacity data. For comparison, the zero-field critical entropy fraction amounts to 0.20 in the case of the quasi-ideal three-dimensional Heisenberg magnet EuS [3].

5.2. $EuDy_2O_4$

There are two sets of measurements of the heat capacity for $EuDy_2O_4$, with some overlap (Fig. 5). For $B \geq 1$ T ($B \leq 2$ T), the data have been measured in a ^{4}He (^{3}He) cryostat, i.e., above 2 K (0.35 K). The zero-field data can nicely be extrapolated to $T \to 0$ by a $AT^{3/2}$ law, hence allowing to obtain the absolute entropy, using Equation 1. Note that the heat capacity of $EuDy_2O_4$ is completely different from that of $EuGd_2O_4$. The Dy compound has two sharp transitions at T_{C1} = 3.65 ± 0.05 K and T_{C2} = 4.7 ± 0.1 K. Both peaks fade out for weak fields, which indicates ferro- or ferrimagnetism, in consonance with the χ_m data. The existence of two peaks in $C_{p,B}$ with similar high entropy content indicates two weakly coupled systems, rather than an order-disorder transition followed by an order-order one within a single spin system.

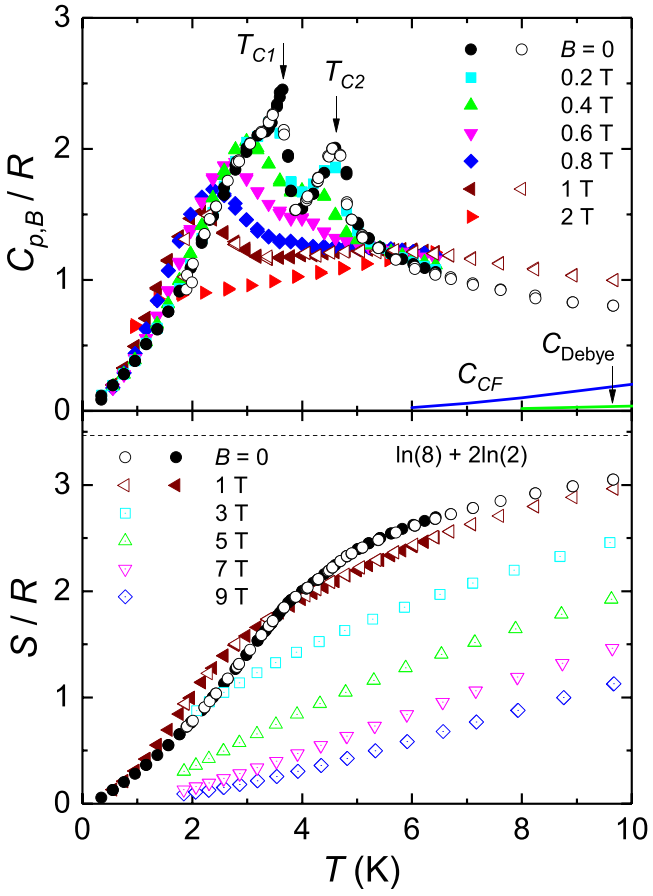

Fig. 5. Temperature-dependence of the molar heat capacity (top) and molar entropy (bottom) of $EuDy_2O_4$, collected with a ^{3}He cryostat (filled symbols) and a ^{4}He cryostat (open symbols) for selected B values, as labelled. Only the low-field $C_{p,B}$ data are plotted for clarity. Shown also are the contributions of excited crystal-field levels (blue line) and of the lattice, calculated from the Debye model (green line). The dashed line is the high-temperature limit of the magnetic entropy of one $s = 7/2$ spin and two $s = 1/2$ effective pseudo-spins per formula unit, i.e., $S_m(T \to \infty)/R = \ln(8) + 2\ln(2) = 3.47$.

The contribution to $C_{p,B}$ of the thermal population of the crystal field levels has been computed from the experimental data of $SrDy_2O_4$, determined by inelastic neutron scattering [27]. The crystal field splits the free Dy^{3+} ion manifold into 8 Kramers doublets. The magnitude of the splitting is different for Dy1 and Dy2, in such a way that the heat capacity of the excited crystal-field levels (C_{CF}) is negligible for Dy2 in the temperature range of our study. The contributing C_{CF} is mainly due to Dy1 crystal-field excited levels, but it is significant only above 7 K (Fig. 5).

The zero-field entropy (Fig. 5, bottom panel) remains well below the limit of one spin $s = 7/2$ (Eu) and two pseudo spins $s = 1/2$ (Dy1

and Dy2) per formula unit, for temperatures well above T_{C2}. This behavior indicates short-range order, as typically encountered in a frustrated or low-dimensional system. In regard to which sublattice produces the peak at T_{C1} or T_{C2}, it is difficult to separate the heat capacity or entropy of each subsystems, even for zero field. One could be tempted to ascribe one peak to Eu and the other to Dy, but the experiment shows that the peaks have similar entropy contents, while they should rather be 3/2 times larger for Eu with respect to both Dy together. This point will be discussed further in Section 7.

6. Magnetocaloric effect

The isothermal entropy variation ΔS_T, for the applied magnetic field change $\Delta B = B - 0$, is obtained in the following three ways.

- From magnetization data, integrating the Maxwell relation

$$\left(\frac{\partial S}{\partial B}\right)_T = \left(\frac{\partial M}{\partial T}\right)_B \Rightarrow$$
$$\Delta S_T(T, \Delta B) \equiv S(T, B) - S(T, 0) = \int_0^B \left(\frac{\partial M}{\partial T}\right)_B dB. \quad (2)$$

- From heat capacity, via the entropy calculation

$$\Delta S_T(T, \Delta B) = S(T, B) - S(T, 0) =$$
$$S(T_0, B) - S(T_0, 0) + \int_{T_0}^{T} \frac{C_{p,B}(T) - C_{p,0}(T)}{T} dT, \quad (3)$$

where T_0 is a reference temperature at which ΔS_T is known precisely. If $C_{p,B}$ can be extrapolated at $T \to 0$, the simplest option is to take $T_0 = 0$, otherwise additional data or a theoretical estimation of $\Delta S_T(T_0, B)$ are necessary.

- From direct measurements, carried out for $EuDy_2O_4$, as detailed in A.

The refrigeration capacity (RC), i.e., the amount of heat transferred between cold (at T_1) and hot (at T_2) sinks in an ideal refrigeration cycle, for $\Delta B = B - 0$, is calculated as

$$RC(\Delta B) = -\int_{T_1}^{T_2} \Delta S_T(T, \Delta B) dT, \quad (4)$$

where the limiting T_1 and T_2 are obtained as the temperatures at the half maximum of the $-\Delta S_T(T, \Delta B)$ curve.

Lastly, the adiabatic temperature variation ΔT_{ad}, for $\Delta B = B - 0$, is obtained from heat capacity, via the entropy calculation, as $\Delta T_{ad}(T, \Delta B) = T' - T$ for any $S(T, 0) = S(T', B)$, that is, T is the initial and T' the final temperature of the adiabatic magnetization $0 \to B$ or, equivalently, T' is the initial and T the final temperature of the adiabatic demagnetization $B \to 0$.

6.1. $EuGd_2O_4$

Fig. 6 shows the values of ΔS_T and ΔT_{ad} obtained for $EuGd_2O_4$ and $EuDy_2O_4$. The Gd compound has an outstanding MCE, with maximum values of $-\Delta S_T = 37.1$ Jkg^{-1}K^{-1} at $T = 7.0$ K, which corresponds to RC = 511.3 Jkg^{-1}, and $\Delta T_{ad} = 17.1$ K at $T = 10.2$ K, for a field variation

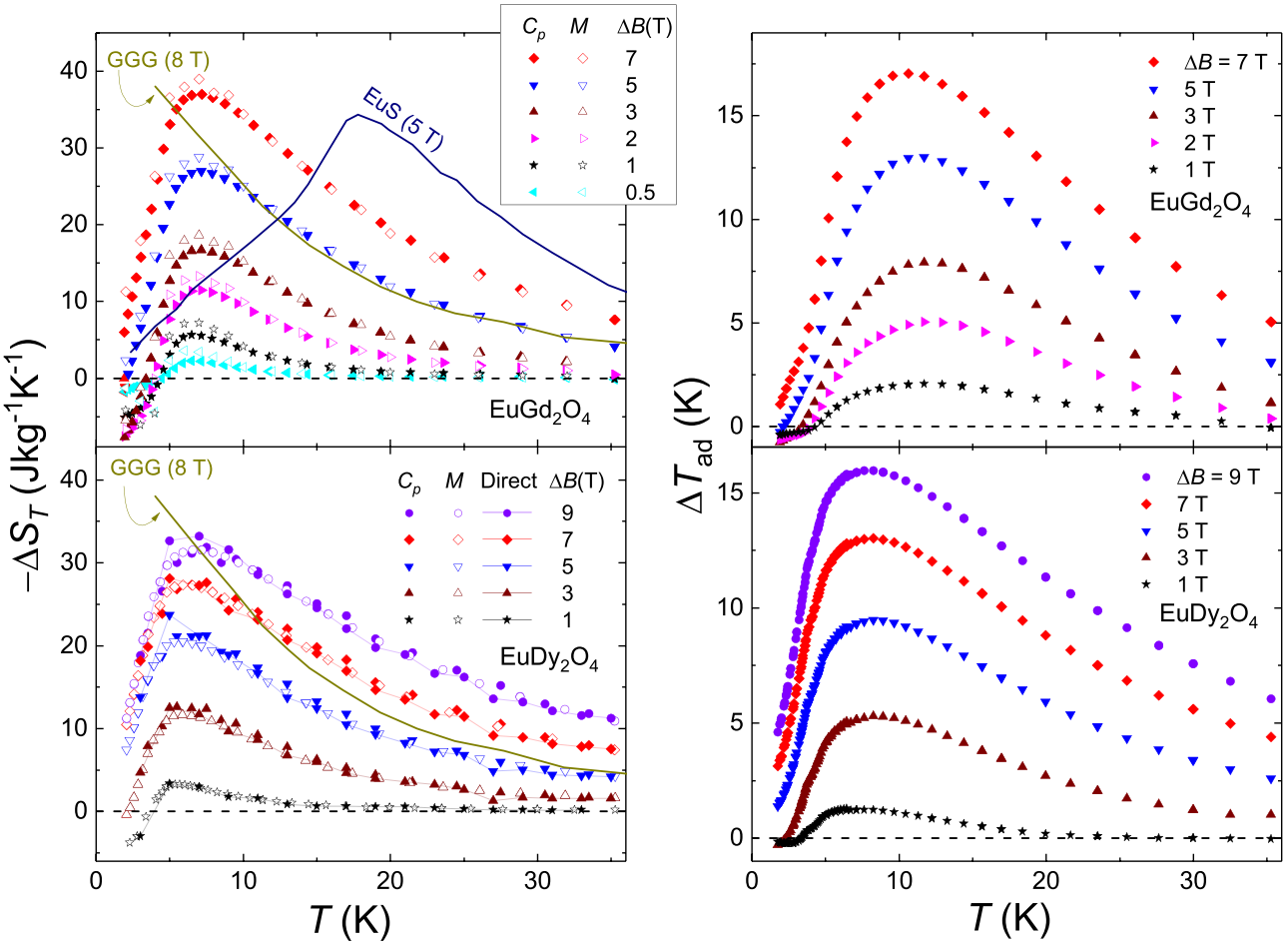

Fig. 6. Temperature-dependence of the isothermal entropy variation (left) and adiabatic temperature variation (right) for $EuGd_2O_4$ (top) and $EuDy_2O_4$ (bottom), obtained from isothermal magnetization (open symbols) and heat capacity (filled symbols) data, in addition to direct measurements (linked symbols), for several applied field changes $\Delta B = B - 0$, as labelled. Isothermal entropy variation data for ferromagnetic EuS (for 5 T, from Ref. [3]) and paramagnetic GGG (for 8 T, from Ref. [1]) are also shown for comparison.

from 0 to 7 T. The effect of high magnetic density is evident when $SrGd_2O_4$ reaches only a maximum of $-\Delta S_T = 27$ $Jkg^{-1}K^{-1}$ at 3 K, for the same fields [25]. These results can be also compared to those of the reference compounds EuS and GGG. The ferromagnetic EuS has a much larger MCE at its T_C, but $-\Delta S_T$ of EuS decays significantly at lower temperatures, becoming smaller than in $EuGd_2O_4$ for temperatures below ca. 12 K. The paramagnetic GGG has a strong MCE at very low temperature. Above 7 K, its $-\Delta S_T$ for 8 T almost overlap with that of $EuGd_2O_4$, but for 5 T. Considering that $-\Delta S_T$ is proportional to B^2 at high temperature, this fact means that the present compound multiplies the MCE of GGG by $(8/5)^2 \approx 2.6$. Below T_{C1} and for low applied fields, ΔS_T is positive and ΔT_{ad} is negative, as expected for an antiferromagnet below the spin-flop field.

6.2. $EuDy_2O_4$

The isothermal entropy variation of $EuDy_2O_4$ (Fig. 6) has been determined directly and from magnetization and heat capacity measurements. The direct measurements can be considered exact within ± 0.5 $Jkg^{-1}K^{-1}$ and the values obtained at 30.5 K were used to obtain the absolute entropies for high fields, rather than using the extrapolation for $T \rightarrow 0$ of the heat capacity that gives worse precision. Although the values of ΔS_T are generally lower than those for $EuGd_2O_4$, they still reach a respectable 27.8 $Jkg^{-1}K^{-1}$ at $T = 6.1$ K, which corresponds to RC = 393.6 Jkg^{-1}, for a field variation from 0 to 7 T, which is notably higher than ΔS_T of, e.g., GGG for 8 T and above 10 K. This ΔS_T value is also higher than the maximum reached by $SrGd_2O_4$ for the same field variation, at 3 K [25]. For the same field variation of $\Delta B = 7$ T, the maximum value of the adiabatic temperature change is $\Delta T_{ad} = 13.0$ K at $T = 8.1$ K. Increasing ΔB to 9 T leads to maxima of $-\Delta S_T = 33.3$ $Jkg^{-1}K^{-1}$ at $T = 7.0$ K, which corresponds to RC = 567.4 Jkg^{-1}, and $\Delta T_{ad} = 16.1$ K at $T = 8.2$ K. The fact that two Gd^{3+} ions per formula unit, as in $SrGd_2O_4$, contribute less than the two Dy^{3+} and one Eu^{2+} ions in $EuDy_2O_4$ suggests that Dy^{3+} spin states other than $s = 1/2$ are thermally populated at zero applied field.

7. Discussion

The magnetic properties of $EuLu_2O_4$, where Lu^{3+} has no magnetic moment, can be explained as due to a ferromagnetic exchange interaction between the nearest Eu^{2+} ions, lying in chains perpendicular to the *m* plane of the *Pnam* space group (Fig. 1), with a much weaker antiferromagnetic interchain interaction [26]. Therefore, there is a moderate spin-flop (or spin-flip) field, estimated to be 2 T. The easy direction of the magnetic moments is perpendicular to the mirror plane *m* (*c*-axis), likely determined by dipolar interactions. Differently in the series AR_2O_4, with *A* = Sr or Ba being a nonmagnetic alkaline-earth ion, the interaction is antiferromagnetic and there is not long-range magnetic order or it sets up at lower temperatures than accessed, well below 1 K, i.e., smaller than the respective Curie-Weiss constants. This behavior is clearly due to the frustration of the antiferromagnetic interactions, although the Curie-Weiss law has not necessarily to be obeyed by all rare-earth ions, when the thermal population of the excited crystal-field levels changes the magnetic moment with temperature. The simplest cases are, on an extreme, the quasi-isotropic Gd^{3+} and, on the other extreme, the strongly uniaxial rare-earths Dy^{3+} or Ho^{3+} that can be considered as quasi-ideal Ising pseudo-spins 1/2.

7.1. $EuGd_2O_4$

The presence of the magnetic and isotropic ion Eu^{2+} changes abruptly the behavior of EuR_2O_4. For the Gd compound, the susceptibility and magnetocaloric effect show a Curie-Weiss behavior at high temperature, although the system orders antiferromagnetically at $T_N = 4.6$ K, as for the Lu compound. Most likely, the ferromagnetic intrachain interaction between Eu^{2+} ions is dominant in the paramagnetic state, while the presence of Gd^{3+} ions reinforces antiferromagnetic correlations between chains. The proposed magnetic structure is formed by antiparallel-stacked ferromagnetic chains oriented along the *c*-axis (see Fig. 1 and Ref. [26]). The Gd^{3+} ions order in ladders that run parallel to the Eu chains. Within each ladder, the two Gd chains would align antiparallel to one another, resulting in one of the lowest energy configurations for the frustrated intraladder antiferromagnetic interaction. Notably, this structure is compatible with all experimental data, i.e., susceptibility, heat capacity and magnetocaloric effect.

We developed a mean-field calculation B.2 for the six sublattices indicated in Fig. 1, namely, A and D for Gd1, B and E for Gd2, C and H for Eu, all of them isotropic. The average moments either are along or opposite to the external field, a spin-flop phase is considered. A good agreement with the experiments can be found for $J_{CC} = J_{AC} = J_{BC} = 0.5$ K, $J_{AA} = J_{AD} = J_{BE} = -0.2$ K, and $J_{AE} = J_{BD} = J_{BH} = J_{CE} = -0.1$ K, and all other constants being zero. Several features observed in the experiments are also predicted by the model. For instance, the simulated system orders at $T_N = 5.1$ K in the aforementioned magnetic structure. Furthermore, the calculated susceptibility obeys the Curie-Weiss law with $\theta = -4$ K, as for a ferromagnet, and it decreases below T_N. Unfortunately, mean-field approximation does not take into account short-range order. Therefore, the calculated heat capacity drops quickly to zero above T_N, the entropy at low fields is much higher than experimentally observed, and so is the simulated $|\Delta S_T|$.

7.2. $EuDy_2O_4$

The aforementioned spin configuration was proposed as the most probable for all EuR_2O_4 compounds in the series [26], but $EuDy_2O_4$ is more complicated. Neutron diffraction experiments and crystal-field calculations for SrR_2O_4 show that the Dy1 moments are in the *ab*-plane (mirror plane) and Dy2 moments in the *c* direction [27]. The crystal-field splitting for both sites is much higher than k_BT below 10 K (Fig. 5 shows the contribution to the heat capacity of the excited crystal-field levels). Therefore, Dy1 and Dy2 behave as Ising systems with pseudo-spin 1/2, but perpendicular to one another. The exchange interaction is virtually zero, since the energy interaction Dy1-Dy2 does not change if all spins of one sublattice are inverted. It follows that each Dy sublattice behaves as independent, hence explaining the existence of the two magnetic transitions, revealed by $C_{p,B}$ data (Fig. 5).

The nearest neighbors to Eu are two Dy2 ions at distances of 3.31 Å and 3.36 Å, respectively, marked by green links in Fig. 1, and only one Dy1 at a longer distance of 3.57 Å, marked by red links in the same figure. All the three neighbors lie on the same *m* plane of the *Pnam* space group. The shortest Eu-Eu distance is 3.43 Å along the chain, parallel to the *c*-axis. The Eu-Dy2 distance is shorter than the Eu-Dy1 one and each Eu has two nearest Dy2 neighbors. An antiferromagnetic Eu-Dy interaction, in addition to the ferromagnetic Eu-Eu exchange (and dipolar) interaction, would explain a ferrimagnetic ordering of the Eu, Dy2 sublattices along the *c*-axis, and, ultimately, the transition at T_{C2}.

To gain insight on the magnetic ordering mechanism, specifically for T_{C1}, we developed a mean-field calculation B.1 for three sublattices, namely, A, B, and C, respectively for Dy2, Dy1, and Eu atoms, characterized by $s_A = s_B = 1/2$, $g_A = g_B = 20$ and $s_C = 7/2$, $g_C = 2$. A is fixed along the *z*-axis, B along the *x*-axis and C is isotropic. The only non-zero exchange constants we set for this simplified model are $J_{AC} = -3.3$ K, $J_{BC} = -3.0$ K, and $J_{CC} = 0.30$ K, with $J_{ij} > 0$ meaning ferromagnetic exchange. With these parameters, the observed transition

temperatures are well reproduced, so are the dependencies of magnetization, susceptibility and heat capacity with temperature and field, but, of course, not the entropy above T_{C2}. At zero field and decreasing temperature, sublattice C is antiparallel to A just below T_{C2}, with B still disordered. Below T_{C1}, the angle between C and A increases with decreasing temperature, reaching ca. 45º at $T = 0$. The entropy at T_{C1}, i.e., $S(T_{C1})/R$, is a large fraction of the total entropy, as it also happens in the experiment. The A and B sublattices have minor contributions to the entropy. This explains why both heat capacity experimental peaks have similarly high entropy contents, since both anomalies can count with an important contribution of the Eu atoms. The peak at T_{C2} is ascribed to the mechanism of magnetic order involving Dy2 spins, together with the *z*-component of the Eu spins. Just below T_{C2}, there is still a considerable disordered component in the *x*-plane that orders progressively with Dy1. A similar behavior has been observed in other compounds, like $GdCrO_4$ [5], although in this case the perpendicular component of the Gd moments order because of the direct Gd-Gd exchange, while the Cr-Cr and Gd-Cr interactions order the Cr spins along the *c*-axis and the parallel component of the Gd spins at a relatively high temperature $T_C = 21.3$ K. For $GdCrO_4$, the Gd-Gd interaction is much weaker than Gd-Cr and produces the ordering of the perpendicular component at the much lower temperature of $T_N = 4.6$ K, below which, the parallel component is nearly saturated. Therefore, the entropy content of the anomaly is very small at T_N.

Further exploring the mean-field simulation, we observe that the net moment along the field direction (DC susceptibility) decreases at low temperatures and low fields, similarly as in the experiments. Magnetic saturation is reached for fields stronger in the simulation (e.g., $\mu_z = 16\mu_B$ for $B_z = 3$ T) than in the experiments (Fig. 2, bottom panel). Regardless, the magnetic moment of $\mu = 18\mu_B$, experimentally observed for 2 K and 9 T, corresponds well with sublattices A and C parallel to the field, i.e., $(g_A s_A + g_C s_C)\mu_B = 17\mu_B$, with an extra small contribution from sublattice B that would be nearly perpendicular to the field.

8. Conclusions

$EuGd_2O_4$ and $EuDy_2O_4$ differ significantly from one another in terms of their magnetic and magnetocaloric properties. However, both materials have a strong magnetocaloric effect due to a higher density of magnetic moments than in SrR_2O_4 or BaR_2O_4 (*R* = rare earths). Given that the *R*-*R* exchange is antiferromagnetic and frustrated, the magnetic behavior depends mainly on the Eu-*R* exchange. For $EuGd_2O_4$, the magnetization and heat capacity data below $T_N = 4.6$ K are supported by our mean-field simulation and consistent with the antiferromagnetic configuration proposed in Ref. [26]. Above T_N, the ferromagnetic Eu-Eu interaction takes the dominant role, leading to a negative Curie-Weiss constant and, ultimately, to an increase of the MCE with respect to an equivalent paramagnet. The isothermal entropy variation of $EuGd_2O_4$ reaches the maximum $-\Delta S_T = 37.1$ $Jkg^{-1}K^{-1}$ at $T = 7.0$ K, which corresponds to $RC = 511.3$ Jkg^{-1}, while its adiabatic temperature variation reaches the maximum $\Delta T_{ad} = 17.1$ K at $T = 10.2$ K, all of them for a field variation from 0 to 7 T. Its MCE is even larger than that of well-established magnetocaloric materials, like GGG and EuS, for the temperature range between ≈5 K and 15 K, making this material very interesting for applications in cryogenic magnetic refrigeration.

For $EuDy_2O_4$, Dy1 and Dy2 Ising spins form mutually perpendicular sublattices that order at $T_{C1} = 3.65$ K and $T_{C2} = 4.7$ K, respectively. The magnetic ordering mechanism is mainly dictated by the Eu-Eu ferromagnetic interaction, combined with the Eu-Dy1 and Eu-Dy2 antiferromagnetic ones. Mean-field simulation can give a semi-quantitative description of the measured heat capacity and magnetization. The maximum entropy value of this material, corresponding to one Eu^{2+} spin $s = 7/2$ and two Dy^{3+} effective pseudo-spins $s = 1/2$ per formula unit, is calculated as $S = [2\ln(2) + \ln(8)]R = 3.47R = 53.3$ $Jkg^{-1}K^{-1}$. However, the antiferromagnetic correlations, the strong Dy anisotropy and the perpendicular alignment of the Dy1 and Dy2 sublattices, which reduces the net magnetization, impose a limitation to the isothermal entropy variation that, ultimately, reaches the more modest, yet large, values of $-\Delta S_T = 27.8$ $Jkg^{-1}K^{-1}$ at $T = 6.1$ K, $RC = 393.6$ Jkg^{-1} and $\Delta T_{ad} = 13.0$ K at $T = 8.1$ K, for varying B from 0 to 7 T, and $-\Delta S_T = 33.3$ $Jkg^{-1}K^{-1}$ at $T = 7.0$ K, $RC = 567.4$ Jkg^{-1} and $\Delta T_{ad} = 16.1$ K at $T = 8.2$ K, for varying B from 0 to 9 T.

We foresee that other EuR_2O_4 compounds will be the subject of future investigations. One of the reasons is because both *R* ions might have the same direction for the uniaxial anisotropy, likely resulting in an even stronger MCE. Besides, anisotropic MCE attracts considerable interest because it allows cooling by rotating the sample in static magnetic fields [35–37].

CRediT authorship contribution statement

E. Palacios: Conceptualization, Methodology, Investigation, Writing - Original Draft, Supervision, Funding acquisition. **R. Sáez-Puche:** Investigation, Funding acquisition. **J. Romero:** Investigation. **Y. Doi:** Investigation, Resources. **Y. Hinatsu:** Investigation, Resources. **M. Evangelisti:** Methodology, Investigation, Writing - Review & Editing, Visualization, Supervision, Funding acquisition.

Declaration of Competing Interest

The authors declare that they have no known competing financial interests or personal relationships that could have appeared to influence the work reported in this paper.

Acknowledgments

This work has been funded by Spanish Ministry of Science and Innovation (Projects MAT2017–86019-R, MAT2017–84385-R, RTI2018–098537-B-C22), Gobierno de Aragón (Consolidated Group E11_20R) and Comunidad de Madrid (Project S2009/PPQ-1626). Authors would like to acknowledge the use of the Servicio General de Apoyo a la Investigación-SAI, Universidad de Zaragoza. This work is devoted to our colleague and friend Prof. Emilio Morán, Universidad Complutense de Madrid, recently deceased of COVID-19.

Appendix A. Direct determination of ΔS_T

Fig. A.7 shows schematically the set-up employed for the direct measurement of the isothermal entropy variation ΔS_T. The sample is glued on a Al_2O_3 plate by a highly thermal conducting grease, namely, Apiezon N. On the bottom side, there is a calibrated resistance thermometer connected electrically to a 4-point ohmmeter and thermally to a bath at constant, controlled temperature T_0. The wires also serve for mechanical support of the plate. Heat diffusion of Al_2O_3 can be considered infinite in the temperature range of the experiments, $2\,K < T < 50\,K$.

When the temperature of the sample is $T \neq T_0$, there is a heat flux $\dot{Q} = k(T_0 - T)$ from the bath, where k is the conductance of the wires measured separately in a calibration run, using a sample of oxygen-free copper. For the measurement of ΔS_T, a magnetic field is quasi-statically varied at a typical rate of 0.01 T/s. Therefore, the time evolution of the entropy change of the sample is

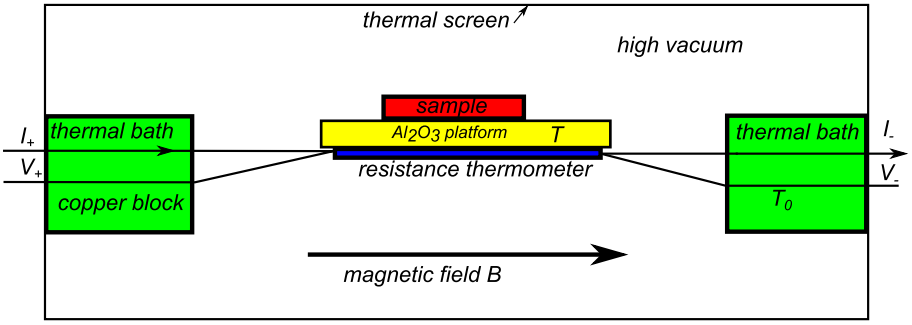

Fig. A.7. Scheme of the set-up for the direct determination of ΔS_T.

$$\Delta S(t) = \int_0^t \frac{\dot{Q}}{T} dt' = \int_0^t \frac{k(T)(T_0 - T)}{T} dt'. \tag{A.1}$$

Fig. A.8 shows an example of a $\Delta S(t)$ measurement for $EuDy_2O_4$. The conductance k is essentially proportional to $(T+T_0)/2$ and for $T_0 > 2\,K$, $|T_0 - T|$ is of some tens of mK. Therefore, the process is quasi-isothermal. In Fig. A.8, $\Delta S_T > 0$ for low fields (inverse MCE) and $\Delta S_T < 0$ for high fields (normal MCE). The change in the slope of $\Delta S(t)$ is evident on demagnetization and has been assigned to a spin-flip transition at a field of $B_{sf} \simeq 0.8\,T$, in good agreement with the estimation of 0.7 T given in Section 4.2. For a precise determination of ΔS_T, the field variation is stopped at several desired values, leaving T to relax to T_0. When the final temperature is rigorously equal to the initial one, the entropy variation is entirely ascribed to the sample, without any effect of the addenda. This technique allows to study transitions at constant temperature. It is also possible to study irreversibility processes, revealed by a net heat release in an isothermal magnetization demagnetization cycle (e.g., hysteresis), or cases in which the final state is different from the initial one, for the same temperature and field.

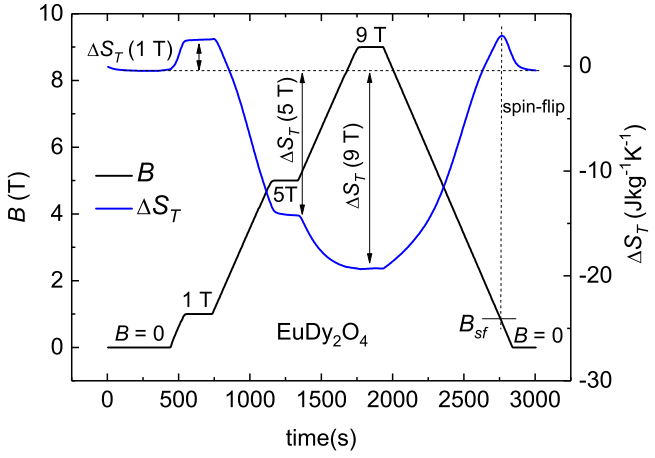

Fig. A.8. Time evolution of ΔS_T for a quasi-isothermal magnetization-demagnetization cycle for $EuDy_2O_4$.

B. Mean-field calculations

B.1. $EuDy_2O_4$

We aim at testing the spin arrangements proposed in the main text and, for the sake of simplicity, we first consider the case of $EuDy_2O_4$. Within a mean-field (MF) approximation, we model this system as consisting of three sublattices, namely, A and B made of Ising spins with directions parallel to z and x, respectively, and perpendicular to one another, and C with isotropic spins that can point in any direction within the xz-plane. The exchange constant between a spin in sublattice i and the nearest neighbors in sublattice j is symbolized as J_{ij}. Since sublattices A and B are frustrated in $EuDy_2O_4$, only J_{AC}, J_{BC} and J_{CC} are considered nonzero, to reduce the number of free parameters. If $\mathbf{B} = (B_x, 0, B_z)$ is the external magnetic field, the corresponding mean fields are:

$$\begin{aligned} B_A &= B_z + (J_{AA} s_A \sigma_A + J_{AC} s_C \sigma_C \cos\phi)/(g_A \mu_B) \\ B_B &= B_x + (J_{BB} s_B \sigma_B + J_{BC} s_C \sigma_C \sin\phi)/(g_B \mu_B) \\ B_{Cx} &= B_x + (J_{CC} s_C \sigma_C \sin\phi + J_{BC} s_B \sigma_B)/(g_C \mu_B) \\ B_{Cz} &= B_z + (J_{CC} s_C \sigma_C \cos\phi + J_{AC} s_A \sigma_A)/(g_C \mu_B), \end{aligned} \tag{B.1}$$

where $\sigma_i = \langle \mu_i \rangle / \mu_{i,s}$ is the ratio of the thermal average of the moment at site i to the saturation $\mu_{s,i} = g_i \mu_B s_i$, and $\phi = \arcsin(B_{Cx}/B_C)$ with $B_C = \sqrt{B_{Cx}^2 + B_{Cz}^2}$. Defining the dimensionless variable $x_i = g_i s_i \mu_B B_i/(k_B T)$, the three MF equations are

$$\sigma_i = B_{s_i}(x_i),\ i = \text{A, B, C}, \tag{B.2}$$

where $B_s(x)$ is the Brillouin function for spin s. The set of equations B.1 and B.2 can be solved iteratively on decreasing temperature, with initial seed σ_i given by the Curie law, or on increasing temperature, starting with the minimum energy configuration. Equations B.1 and B.2 frequently have several solutions (the most evident for $B = 0$ is $\sigma_i = 0$ at any temperature) and the iteration procedure leads to one of them, depending on the trial starting value. The lowest free-energy solution is determined at every temperature and the thermodynamic functions are then computed, following the standard MF approach.

At zero applied field, the experimentally observed ordering temperatures T_{C2} and T_{C1} identify nicely with $T_{CA} = 4.65$ K and $T_{CB} = 3.89$ K, respectively, which are calculated for $J_{AC}/k_B = -3.3$ K, $J_{BC}/k_B = -3.0$ K and $J_{CC}/k_B = 0.3$ K (Fig. B.9, top panel). The larger values of the calculated heat capacity below the ordering temperatures, with respect to the experimental result shown in Fig. 5, can be well explained by the presence of short-range order in $EuDy_2O_4$, which cannot be accounted for by the MF model. On decreasing temperature between T_{CA} and T_{CB}, the

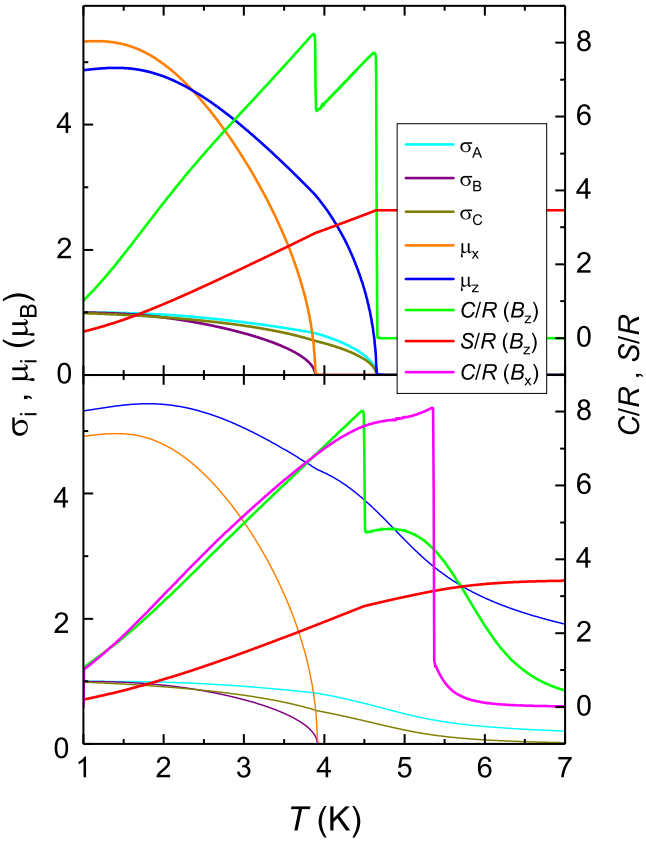

Fig. B.9. For $EuDy_2O_4$, mean-field calculation, at zero external field (top) and for $B_x = 0$, $B_z = 0.2$ T (bottom), of a three-sublattice ferrimagnet with moments of sublattice A along the z-axis, B along the x-axis and C isotropic. Left scale: Magnetization $\langle \mu_i \rangle$ and polarization $\sigma_i = \langle \mu_i \rangle / \mu_{is}$, where μ_{is} is the saturation of the sublattice i = A, B, C. Right scale: Magnetic heat capacity at constant field C_B/R and entropy S/R. μ_{Cz} is opposite to μ_A below T_{CA}, and μ_{Cx} to μ_B below T_{CB}, within the analyzed temperature range.

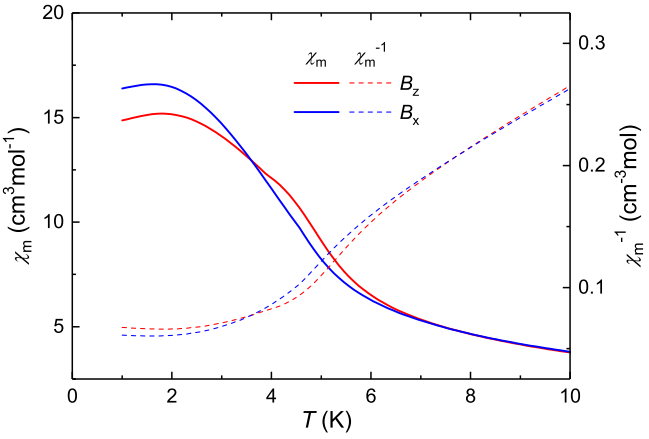

Fig. B.10. For $EuDy_2O_4$, molar magnetic susceptibility (left) and its inverse (right), obtained from the mean-field model for three sublattices A, B and C, for a magnetic field of 0.2 T applied along the x and y directions, as labelled.

magnetization of sublattice B is zero and that of sublattice C is opposite to that of sublattice A, both in the z-direction. Below T_{CB}, the magnetization of sublattice B increases and that of sublattice C develops an x-component, opposite to it. This component forms a variable angle with the z-axis, which nearly reaches 45^o (since $J_{AC} \simeq J_{BC}$) at $T = 0$, i.e., when sublattices A and B are fully ordered. Note that the model predicts two transitions, even if the interactions A-C and B-C are of similar intensity. This point is endorsed by the group theory applied to the Landau expansion. The ordering of the A and B perpendicular sublattices corresponds to different irreducible representations. If both sublattices were parallel, they would correspond to the same representation and would order together, as occurring in $EuGd_2O_4$. There, the absence of magnetic anisotropy facilitates the polarization of the moments along the field direction.

The heat capacity anomaly at T_{CA} becomes rounded as a field is applied along the z-direction (Fig. B.9, bottom panel), so does the anomaly at T_{CB} as the field is applied along the x-axis. Above T_{CA} and in the temperature range shown in Fig. B.9, the average moment of sublattice C is antiparallel to sublattices A or B, depending on field direction. At higher temperatures, the polarization is very small and the exchange field is negligible with respect to the external field. For instance, for $B_z = 0.2$ T and $B_x = 0$, the moments of sublattices A and C orient parallel to the field above 8.2 K and the susceptibility χ obeys a Curie-Weiss law with positive θ. A similar behavior is also obtained for B in the x-direction (Fig. B.10).

B.2. $EuGd_2O_4$

For modeling the properties of $EuGd_2O_4$, we consider a system of 6 sublattices, namely, A and D for Gd1, B and E for Gd2, C and H for Eu. All spins are treated as isotropic. The thermal average moments are oriented either parallel or antiparallel with respect to the external field, **B** (z-axis). There are 21 different exchange constants between nearest neighbors, which can be reduced by symmetry to those indicated by different types of links in Fig. 1.

The mean field at site i is

$$B_i = B + \frac{1}{g_i \mu_B} \sum_{\beta} J_{ij} s_j \sigma_j, \tag{B.3}$$

for every i, j = A, B, C, D, E, H. The average moment is computed iteratively using equations B.2 and B.3 for the 6 sublattices. The partition function and other thermodynamic functions are computed in the same manner as for $EuDy_2O_4$. The exchange constants J_{ii} represent the intra-chain interactions and several symmetry relations can be identified, namely, $J_{ij} = J_{ji}$, $J_{DD} = J_{AA}$, $J_{EE} = J_{BB}$, $J_{HH} = J_{CC}$, $J_{AC} = J_{DH}$, $J_{BC} = J_{EH}$. Fitting all the remaining free constants using the experimental data is impossible. Therefore, a simplification is made, based on the pseudo-symmetry (similar distances) of the crystal lattice, that is, $J_{CC} = J_{AC} = J_{BC} > 0$, $J_{AA} = J_{AD} = J_{BE} < 0$, $J_{AE} = J_{BD} = J_{BH} = J_{CE} < 0$, and any other exchange is taken as zero. This set of exchange constants corresponds to a ferromagnetic (antiferromagnetic) interaction between each Eu^{2+} ion and its nearest Eu^{2+} (Gd^{3+}) ion.

A good agreement with the experimental data is obtained for $J_{AA} = -0.1$ K, $J_{CC} = 0.5$ K and $J_{AE} = -0.1$ K. These interactions produce an antiferromagnetic configuration at low temperature and zero field, where sublattices A, B, and C point up and sublattices D, E, and H down, as shown in Fig. 1. The magnetic polarization of each sublattice is drawn in Fig. B.11 (top panel), together with the susceptibility of the system (middle panel) that follows the Curie-Weiss law at high temperature, with $\theta \simeq -4$ K, as proper of a ferromagnet and in agreement with experimental observation. The ordering temperature is computed to occur at $T_N = 5.1$ K, also in close agreement with experiments. The calculated heat capacity (bottom panel) is more sensitive to the field than the experimental one. Similarly, the calculated entropy increases faster than in the experiments. As for $EuDy_2O_4$, the likely reason of these discrepancies is that short-range order is not taken into account by the MF model, as also evident in the sudden drop of the calculated heat capacity above T_N.

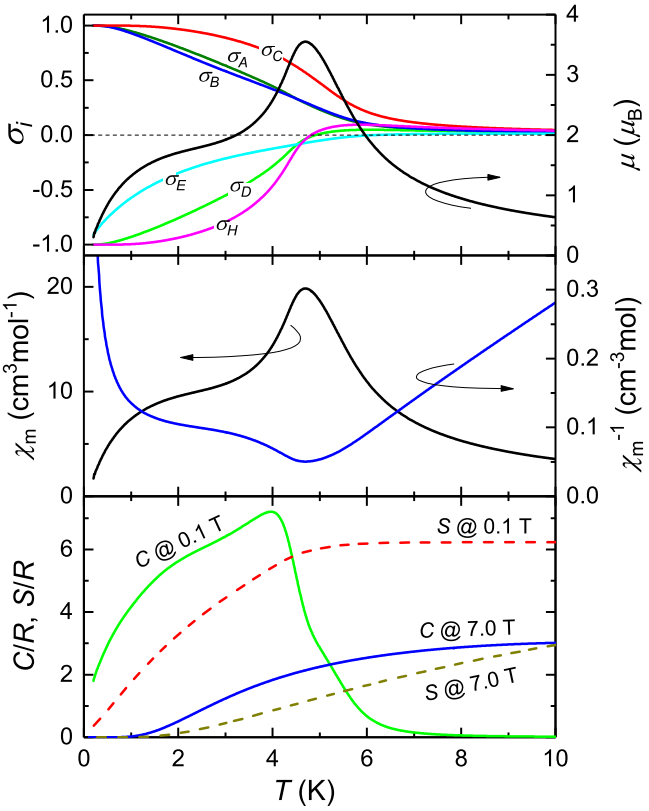

Fig. B.11. For $EuGd_2O_4$, mean-field simulation of the six sublattices. Top: Magnetic polarization σ_i (left scale) and total magnetization (right scale), for an external field $B = 0.1$ T. Middle: Magnetic susceptibility (left) and its inverse (right), for $B = 0.1$ T. Bottom: Magnetic heat capacity (left) and magnetic entropy (right), for $B = 0.1$ and 7.0 T, as labelled.

References

[1] A.M. Tishin, Y.I. Spichkin, The Magnetocaloric Effect and its Applications, IOP Publishing Ltd., Bristol, UK, and Philadelphia, USA, 2003.

[2] T. Hashimoto, T. Numasawa, M. Shino, T. Okada, Magnetic refrigeration in the temperature range from 10 K to room temperature: the ferromagnetic refrigerants, Cryogenics 21 (1981) 647–653, https://doi.org/10.1016/0011-5902275(81)90254-X

[3] K. Matsumoto, L. Li, S. Hirai, E. Nakamura, D. Murayama, Y. Ura, S. Abe, Large magnetocaloric effect in sintered ferromagnetic EuS, Cryogenics 79 (2016) 45–48.

[4] L. Li, S. Hirai, E. Nakamura, H. Yuan, Influences of Eu_2O_3 characters and sulfurization conditions on the preparation of EuS and its large magnetocaloric effect, J. Alloy. Compd. 687 (2016) 413–420, https://doi.org/10.1016/j.jallcom.2016.06.053

[5] E. Palacios, C. Tomasi, R. Sáez-Puche, A.J. Dos Santos-García, F. Fernández-Martínez, R. Burriel, Effect of Gd polarization on the large magnetocaloric effect of $GdCrO_4$ in a broad temperature range, Phys. Rev. B 93 (2016) 064420, https://doi.org/10.1103/PhysRevB.93.064420

[6] E. Palacios, C. Tomasi, R. Sáez-Puche, A.J. Dos Santos-García, F. Fernández-Martínez, R. Burriel, Enhanced magnetocaloric effect by the rare earth polarization due to the exchange with a transition metal. study of GdCrO4, Sol. State Phen. 257 (2017) 139–142, https://doi.org/10.4028/www.scientific.net/SSP.257.139

[7] E. Palacios, M. Evangelisti, R. Sáez-Puche, A.J. Dos Santos-García, F. Fernández-Martínez, C. Cascales, M. Castro, R. Burriel, O. Fabelo, J.A. Rodráguez-Velamazán, Magnetic structures and magnetocaloric effect in RVO_4 (R = Gd, Nd), Phys. Rev. B 97 (2018) 214401, https://doi.org/10.1103/PhysRevB.97.214401

[8] C. Lacroix, P. Mendels, F. Mila (Eds.), Introduction to Frustrated Magnetism, Springer-Verlag, Berlin Heidelberg, Germany, 2011.

[9] M.E. Zhitomirsky, Enhanced magnetocaloric effect in frustrated magnets, Phys. Rev. B 67 (2003) 104421, https://doi.org/10.1103/PhysRevB.67.104421

[10] S.S. Sosin, L.A. Prozorova, A.I. Smirnov, A.I. Golov, I.B. Berkutov, O.A. Petrenko, G. Balakrishnan, M.E. Zhitomirsky, Magnetocaloric effect in pyrochlore antiferromagnet $Gd_2Ti_2O_7$, Phys. Rev. B 71 (2005) 094413, https://doi.org/10.1103/PhysRevB.71.094413

[11] B. Schmidt, P. Thalmeier, N. Shannon, Magnetocaloric effect in the frustrated square lattice J_1–J_2 model, Phys. Rev. B 76 (2007) 125113, https://doi.org/10.1103/PhysRevB.76.125113

[12] J. Schnack, R. Schmidt, J. Richter, Enhanced magnetocaloric effect in frustrated magnetic molecules with icosahedral symmetry, Phys. Rev. B 76 (2007) 054413, https://doi.org/10.1103/PhysRevB.76.054413

[13] J.W. Sharples, D. Collison, E.J.L. McInnes, J. Schnack, E. Palacios, M. Evangelisti, Quantum signatures of a molecular nanomagnet in direct magnetocaloric measurements, Nat. Commun. 5 (2014) 5321, https://doi.org/10.1038/ncomms6321

[14] S. Pakhira, C. Mazumdar, R. Ranganathan, S. Giri, M. Avdeev, Large magnetic cooling power involving frustrated antiferromagnetic spin-glass state in R_2NiSi_3 (R = Gd, Er), Phys. Rev. B 94 (2016) 104414, https://doi.org/10.1103/PhysRevB.94.104414

[15] S. Pakhira, C. Mazumdar, R. Ranganathan, M. Avdeev, Magnetic frustration induced large magnetocaloric effect in the absence of long range magnetic order, Sci. Rep. 7 (2017) 7367, https://doi.org/10.1038/s41598-017-07459-3

[16] S.R. Dunsiger, J.S. Gardner, J.A. Chakhalian, A.L. Cornelius, M. Jaime, R.F. Kiefl, R. Movshovich, W.A. MacFarlane, R.I. Miller, J.E. Sonier, B.D. Gaulin, Low temperature spin dynamics of the geometrically frustrated antiferromagnetic garnet $Gd_3Ga_5O_12$, Phys. Rev. Lett. 85 (2000) 3504–3507, https://doi.org/10.1103/PhysRevLett.85.3504

[17] P. Wikus, E. Canavan, S.T. Heine, K. Matsumoto, T. Numazawa, Magnetocaloric materials and the optimization of cooling power density, Cryogenics 62 (2014) 150–162, https://doi.org/10.1016/j.cryogenics.2014.04.005

[18] H. Karunadasa, Q. Huang, B.G. Ueland, J.W. Lynn, P. Schiffer, K.A. Regan, R.J. Cava, Honeycombs of triangles and magnetic frustration in SrL_2O_4 (L = Gd, Dy, Ho, Er, Tm, and Yb), Phys. Rev. B 71 (2005) 144414, https://doi.org/10.1103/PhysRevB.71.144414

[19] Y. Doi, W. Nakamori, Y. Hinatsu, Crystal structures and magnetic properties of magnetically frustrated systems $BaLn_2O_4$ and $Ba_3Ln_4O_9$ (Ln = lanthanide), J. Phys. Condens. Matter 18 (2005) 333, https://doi.org/10.1088/0953-8984/18/1/024

[20] O.A. Petrenko, G. Balakrishnan, N.R. Wilson, S. de Brion, E. Suard, L.C. Chapon, Low-temperature magnetic ordering in $SrEr_2O_4$, Phys. Rev. B 78 (2008) 184410, https://doi.org/10.1103/PhysRevB.78.184410

[21] T.J. Hayes, G. Balakrishnan, P.P. Deen, P. Manuel, L.C. Chapon, O.A. Petrenko, Coexistence of the long-range and short-range magnetic order components in $SrEr_2O_4$, Phys. Rev. B 84 (2011) 174435, https://doi.org/10.1103/PhysRevB.84.174435

[22] T. Besara, M.S. Lundberg, J. Sun, D. Ramirez, L. Dong, J.B. Whalen, R. Vasquez, F. Herrera, J.R. Allen, M.W. Davidson, T. Siegrist, Single crystal synthesis and magnetism of the $BaLn_2O_4$ family (Ln = lanthanide), Prog. Solid State Chem. 42 (2014) 23–36, https://doi.org/10.1016/j.progsolidstchem.2014.05.001

[23] B.Z. Malkin, S.I. Nikitin, I.E. Mumdzhi, D.G. Zverev, R.V. Yusupov, I.F. Gilmutdinov, R. Batulin, B.F. Gabbasov, A.G. Kiiamov, D.T. Adroja, O. Young, O.A. Petrenko, Magnetic and spectral properties of the multisublattice oxides $SrY_2O_4:Er^{3+}$ and $SrEr_2O_4$, Phys. Rev. B 92 (2015) 094415, https://doi.org/10.1103/PhysRevB.92.094415

[24] E. Hasan, B.W. Southern, Monte carlo study of a geometrically frustrated rare-earth magnetic compound: $SrGd_2O_4$, Phys. Rev. B 96 (2017) 094407, https://doi.org/10.1103/PhysRevB.96.094407

[25] X. Jiang, Z.W. Ouyang, Z.X. Wang, Z.C. Xia, G.H. Rao, Magnetization, ESR and large magnetocaloric effect in zigzag chain $SrGd_2O_4$, J. Phys. D. 51 (2018) 045001, https://doi.org/10.1088/1361-6463/aaa06c

[26] K. Hirose, Y. Doi, Y. Hinatsu, Magnetic properties of $EuLn_2O_4$ (Ln = rare earths), J. Solid State Chem. 182 (2009) 1624–1630, https://doi.org/10.1016/j.jssc.2009.04.001

[27] A. Fennell, V.Y. Pomjakushin, A. Uldry, B. Delley, B. Prévost, A. Désilets-Benoit, A.D. Bianchi, R.I. Bewley, B.R. Hansen, T. Klimczuk, R.J. Cava, M. Kenzelmann, Evidence for $SrHo_2O_4$ and $SrDy_2O_4$ as model J_1–J_2 zigzag chain materials, Phys. Rev. B 89 (2014) 224511, https://doi.org/10.1103/PhysRevB.89.224511

[28] O. Young, G. Balakrishnan, M.R. Lees, O.A. Petrenko, Magnetic properties of geometrically frustrated $SrGd_2O_4$, Phys. Rev. B 90 (2014) 094421, https://doi.org/10.1103/PhysRevB.90.094421

[29] M. Ruminy, E. Pomjakushina, K. Iida, K. Kamazawa, D.T. Adroja, U. Stuhr, T. Fennell, Crystal-field parameters of the rare-earth pyrochlores $R_2Ti_2O_7$ (R = Tb, Dy, and Ho), Phys. Rev. B 94 (2016) 024430, https://doi.org/10.1103/PhysRevB.94.024430

[30] C.J. Ellis, M.J.M. Leask, D.M. Martin, M.R. Wells, Magnetic interactions in antiferromagnetic $DyPO_4$ (zeeman spectra), J. Phys. C: Solid State Phys. 4 (1971) 2937–2944, https://doi.org/10.1088/0022-3719/4/17/024

[31] J.S. Smart, The Néel theory of ferrimagnetism, Am. J. Phys. 23 (1955) 356–370, https://doi.org/10.1119/1.1934006

[32] H. Kojitani, K. Nishimura, A. Kubo, M. Sakashita, K. Aoki, M. Akaogi, Raman spectroscopy and heat capacity measurement of calcium ferrite type $MgAl_2O_4$ and $CaAl_2O_4$, Phys. Chem. Miner. 30 (2003) 409–415, https://doi.org/10.1007/s00269-003-0332-4

[33] T. Maekawa, K. Kurosaki, S. Yamanaka, Thermophysical properties of BaY_2O_4: a new candidate material for thermal barrier coatings, Mater. Lett. 61 (2007) 2303–2306, https://doi.org/10.1016/j.matlet.2006.08.073

[34] L. Holmes, M. Schieber, Magnetic ordering in Eu_3O_4 and $EuGd_2O_4$, J. Appl. Phys. 37 (1966) 968–969, https://doi.org/10.1063/1.1708542

[35] M. Balli, S. Jandl, P. Fournier, M.M. Gospodinov, Anisotropy-enhanced giant reversible rotating magnetocaloric effect in $HoMn_2O_5$ single crystals, Appl. Phys. Lett. 104 (2014) 232402, https://doi.org/10.1063/1.4880818

[36] V. Tkáč, A. Orendáčová, E. Čižmár, M. Orendáč, A. Feher, A.G. Anders, Giant reversible rotating cryomagnetocaloric effect in $KEr(MoO_4)_2$ induced by a crystal-field anisotropy, Phys. Rev. B 92 (2015) 024406, https://doi.org/10.1103/PhysRevB.92.024406

[37] G. Lorusso, O. Roubeau, M. Evangelisti, Rotating magnetocaloric effect in an anisotropic molecular dimer, Angew. Chem. Int. Ed. 55 (2016) 3360–3363, https://doi.org/10.1002/anie.201510468